Hindawi Publishing Corporation
Journal of Nanomaterials
Volume 2011, Article ID 797639, 6 pages
doi:10.1155/2011/797639

Research Article

Synthesis of Bismuth Ferrite Nanoparticles via a Wet Chemical Route at Low Temperature

Yongming Hu,[1,2] Linfeng Fei,[1] Yiling Zhang,[1] Jikang Yuan,[1] Yu Wang,[1] and Haoshuang Gu[2]

[1] *Department of Applied Physics, Materials Research Center, The Hong Kong Polytechnic University, Kowloon, Hong Kong*
[2] *Key Laboratory of Ferro- & Piezoelectric Materials and Device of Hubei Province, Faculty of Physics and Electronic Technology, Hubei University, Wuhan 430062, China*

Correspondence should be addressed to Yu Wang, apywang@inet.polyu.edu.hk and Haoshuang Gu, guhsh583@yahoo.com.cn

Received 28 March 2010; Accepted 21 July 2010

Academic Editor: Jaetae Seo

Nanoparticles (NPs) of multiferroic bismuth ferrite ($BiFeO_3$) with narrow size distributions were synthesized via a wet chemical route using bismuth nitrate and iron nitrate as starting materials and excess tartaric acid and citric acid as chelating agent, respectively, followed by thermal treatment. It was found that $BiFeO_3$ NPs crystallized at ~350°C when using citric acid as chelating agent. Such crystallization temperature is much lower than that of conventional chemical process in which other types of chelating agent are used. $BiFeO_3$ NPs with different sizes distributions show obvious ferromagnetic properties, and the magnetization is increased with reducing the particle size.

1. Introduction

In recent years, much research interest has been drawn to bismuth ferrite ($BiFeO_3$, abbreviated as BFO), which is known to be the only multiferroic compound that exhibits simultaneous ferroelectric and G-type antiferromagnetic orders over a broad range above room temperature (Curie temperature >800°C, Neel temperature = 370°C) [1–6]. As a partially covalent oxide, BFO has a rhombohedrally distorted perovskite structure belonging to a space group of *R3c* [7]. Nevertheless, it exhibits weak magnetism at room temperature due to a spiral magnetic spin cycloid with a periodicity of ~62 nm [4]. So far, most studies on BFO have been performed on two-dimensional epitaxial thin films grown on various substrates [8–11], where epitaxial strain is manifested so as to alter some important properties including crystal lattice structure, polarization, and magnetization. However, more recent approaches are focusing on polycrystals as well as substrate-free nanostructures such as low-dimensional nanostructures, especially zero-dimensional materials like nanoparticles (NPs) [12–17]. Meanwhile, studies on finite size effect of BFO have been carried out by different authors and some interesting properties (e.g., shift of Neel temperature, gas sensing properties, etc.) have been reported [18–22].

Previous studies have demonstrated that synthesis of BFO NPs through a traditional solid-state method produces poor reproducibility and causes formation of coarser powders as well as $Bi_2O_3/Bi_2Fe_4O_9$ impurity phase [4]. Up to date, several chemical routes (e.g. hydrothermal treatment, mechanochemical synthesis method, and sol-gel methodology, etc.) have been successfully employed for fabricating BFO nanoparticles. However, these approaches have certain shortcomings such as impurities in the final products. Ghosh et al. reported a ferrioxalate precursor method to synthesize BFO NPs through solutions of some specific salts at a temperature of 600°C [23]. Despite the efforts made through enhancing sintering temperature to avoid impurities, a small amount of Bi_2O_3 was found in the final product. Han et al. have accomplished the morphologies tunable synthesis of bismuth ferrites using hydrothermal method [24]. The resulting size of BFO NPs was sometimes large (up to several hundred nanometers) although no impurities were found in the final products. Using the same method, Chen et al. prepared pure phase BFO nanocrystallites at 200°C using KOH concentration of 4 M. In this study, impurity phases

of $Bi_2Fe_4O_9$ and $Bi_{25}FeO_{40}$ were easily formed with only a slight change in the KOH concentration [25]. Selbach et al. synthesized BFO NPs through a modified Pechini method using nitrates as metal precursors [26]. Although pure phase BFO was obtained in this study, contaminant produced by decomposition of the precursor was present. Ghosh et al. synthesized nanosized bismuth ferrite using a soft chemical route with tartaric acid as a template material and nitric acid as an oxidizing agent [27]. However, the crystallinity of the resulting BFO NPs was unsatisfactory and the existence of an impure Bi_2O_3 amorphous phase in the host at low temperature product of 400°C was evident. To deal with the issues mentioned above, our recent research suggests that excess tartaric acid and/or citric acid to be added in the solution so that the crystallinity of BFO NPs can be improved. Herein, we reported a general wet chemical route for synthesizing uniform BFO NPs at about 350°C. To our best knowledge, this is the lowest temperature employed in the literature for BFO fabrication with the exception of certain high pressure techniques such as hydrothermal or solvothermal methods. In addition, the magnetic properties were also investigated for BFO NPs with different size distributions.

2. Experimental

All of the reagents were of analytical grade and used without further purification. Following a typical procedure, bismuth nitrate [$Bi(NO_3)_3 \cdot 5\,H_2O$] and iron nitrate [$Fe(NO_3)_3 \cdot 9\,H_2O$] were weighed in stoichiometric proportions and dissolved in deionized water to make a solution with an independent concentration of 0.2 M before adding 20 mL diluted nitric acid (65~68% HNO_3) to the mixture. Then 10 g of citric acid ($C_6H_8O_7$) were added to the solutions as chelating agent. The light-yellow-colored solution was heated under vigorous stirring until no liquid was left in the beaker to form gel deposit. Each beaker with solid deposit was kept in the oven at 150°C for another 2~3 h. Subsequently, powders were quarterly divided and calcined in the oven for 2 h at 350, 450, and 550°C, respectively, to obtain well-crystallized BFO NPs with controllable sizes. For comparison, another group of powders were synthesized by modifying a typical soft chemical route by using excess tartaric acid as chelating agents [27].

The gel (intermediate product) was subjected to thermal analysis in order to determine the subsequent sintering temperature with simultaneous Thermogravimetric Analysis & Differential Scanning Calorimetry (TG-DSC) system (NETZSCH STA 449 C Jupiter). After heat treatment, the sample was characterized using X-ray diffraction (XRD) with a Bruker AXS D8 ADVANCE X-ray diffractometer with Cu Kα radiation ($\lambda = 0.154178$ nm). Fourier transformation infrared (FT-IR) spectra were obtained on a Perkin-Elmer Spectrum one FT-IR spectrometer at a resolution of 4 cm^{-1} with an HgCdTe detector. Transmission electron microscopy (TEM) images and high-resolution transmission electron microscopy (HRTEM) images were obtained on a JEOL 2011 transmission electron microscope at an acceleration voltage of 200 kV. Magnetization measurements were taken on a LakeShore Vibrating Sample Magnetometry (VSM) system.

3. Results and Discussion

The TG/DSC curves of the precipitated and dried powders are carried out and shown in Figure 1. Since tartaric acid and citric acid can form different chelate compounds with Bi^{3+} and Fe^{3+} ions (as schematically shown in Figures 4(a) and 4(b)), different thermal behaviors were observed from the curves. There are four weight-loss segments in both Figures 1(a) and 1(b). It can be seen that the first and last segments are due to the evaporation of crystalline water and the crystallization process of BFO. The major mass loss of the two intermediate segments in tartaric acid precursor are derived from volatilization of excess tartaric acid, decomposition of chelate complex, and a small amount of nitrate. However, in the citric acid precursor, this loss is caused by the decomposition process only. The analysis results provided us a detailed guide to our subsequent heat treatment process, which showed that citric acid precursor has a relatively lower crystallization temperature (indicated by red arrows in Figure 1), that is, nearly 100°C lower than that of the tartaric acid precursor. More importantly, to our best knowledge, a crystallize temperature of about 350°C is far lower than those reported in the literature.

XRD measurements were performed to characterize the crystal structure of the calcined powders. As shown in Figure 2, all the XRD patterns can be indexed to pure rhombohedral perovskite structure, which are in good agreement with the powder data of JCPDS Card number 20-169. After heat treatment at 350°C, the sample from citric acid precursor begins to generate pure phase BFO while another sample from tartaric acid precursor is still of amorphous feature. It is clear that the crystallization of BFO completed at a temperature of 350°C for citric acid precursor while 450°C for tartaric acid precursor, which is in good line with the TG-DSC analysis. Meanwhile, the particle size of BFO changed remarkably after further heat treatment. Calcined at temperatures above 450°C, well-crystallized and pure phase BFO can be obtained for either precursor. As discussed in early literatures, the grain sizes of BFO NPs grow up with increasing the temperature in soft chemical routes [21, 26]. This can be also confirmed by the peak sharpening of XRD curves (data not shown).

The morphology of the calcined BFO nanoparticles was examined on TEM. Typical TEM images are shown in Figure 3. It is clear that the spherical NPs formed from both precursors are sufficiently fine and uniform on copper grid, and the particle sizes are about 12 and 4 nm, respectively. Hardly any aggregation could be found in our samples compared with traditional approaches. The corresponding selected area electron diffraction patterns (as shown in Figures 3(c) and 3(f)) suggest that our NPs are well crystallized, and both can be indexed to pure BFO rhombohedral crystal structure. The HRTEM image of individual BFO NP (Figure 3(b)) clearly shows an interplanar spacing of 2.778 Å, corresponding to the (110) crystal planes. Furthermore, we

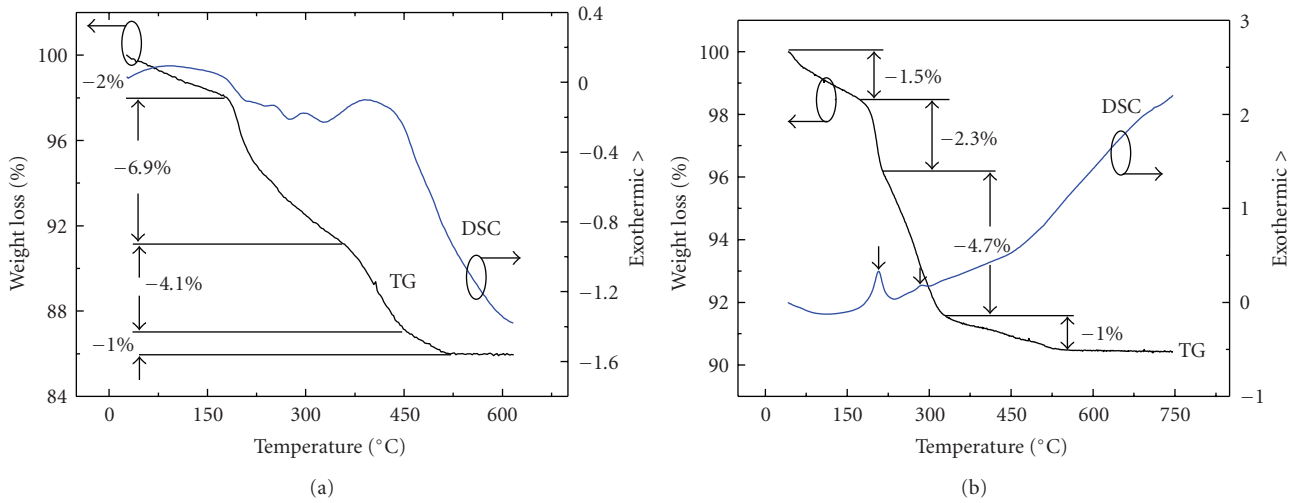

Figure 1: TG-DSC curves of the gel reminders acquired by using (a) tartaric acid and (b) citric acid as chelating agent.

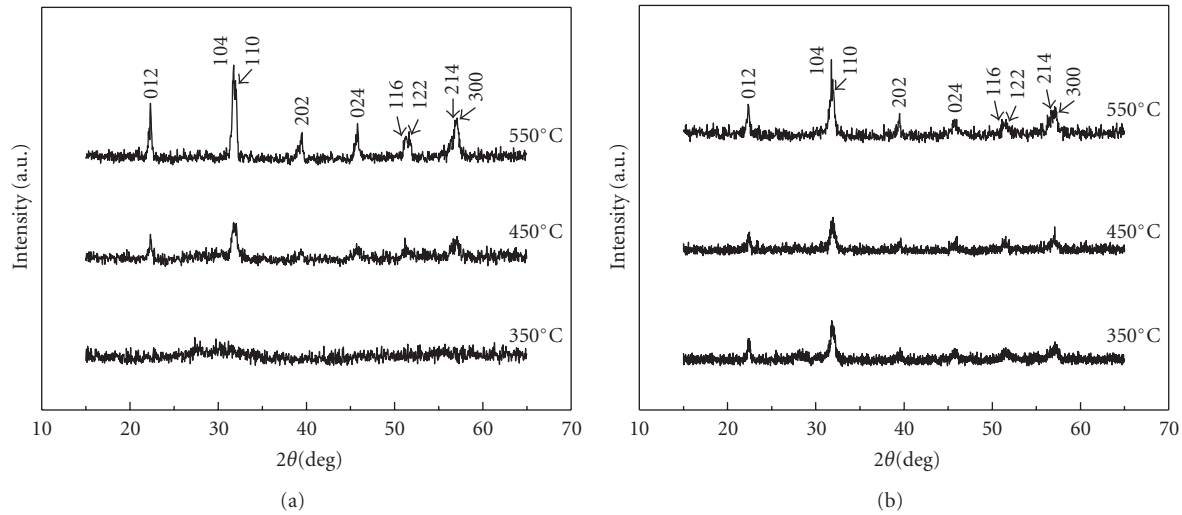

Figure 2: XRD patterns of $BiFeO_3$ samples synthesized by wet chemical route using different chelating agents followed by calcination at 350°C, 450°C and 550°C, respectively. (a) Tartaric acid and (b) citric acid.

can acquire NPs with an average particle size of about 4, 12, 30, and 80 nm through keeping the calcination temperatures at 350, 450, 550, and 650°C, respectively.

Figure 4 shows the FTIR spectra of $BiFeO_3$ precursors using tartaric acid and citric acid as chelating, respectively. As shown, eight characteristic IR peaks appeared for BFO precursor (tartaric acid), while four characteristic IR peaks together with some weak peaks appeared for BFO precursor using citric acid as chelating. Both samples have two sharp and one wide IR peaks, which correspond to the stretching vibrations of C=O and –OH. The IR wide peaks located at 3466 cm^{-1} in (a) and (b) were assigned to the stretching vibrations of structural hydroxyl (OH) groups, and the intense peaks at 1628–1672 cm^{-1} were assigned to the stretching vibrations of C=O (corresponding to the groups of tartaric and citric acid). The IR peaks located at 1374 cm^{-1} were attributed to the symmetry bending vibration of C–H. In addition, a sharp IR peak located at 1278 cm^{-1} was assigned to the stretching vibration of single bond of C–O for tartaric acid precursor sample, while it cannot be observed for citric acid precursor sample. The IR peaks below 1000 cm^{-1} (such as 492, 806, and 902 cm^{-1} for tartaric acid precursor, 477, 551, 613, 858, and 910 cm^{-1} for citric acid precursor) were corresponding to the vibrations bonds of Bi–O or Fe–O, respectively.

A possible mechanism for the formation of BFO NPs was proposed based on previous analysis (as shown in Figure 5). Firstly, $Bi(NO_3)_3 \cdot 5\,H_2O$ and $Fe(NO_3)_3 \cdot 9\,H_2O$ along with chelating agents were added to the deionized water and formed the complex of Bi and Fe (Figures 5(a) and 5(b)). Secondly, sol-like precursor and irregular particles come into being followed by aqueous solution were dried

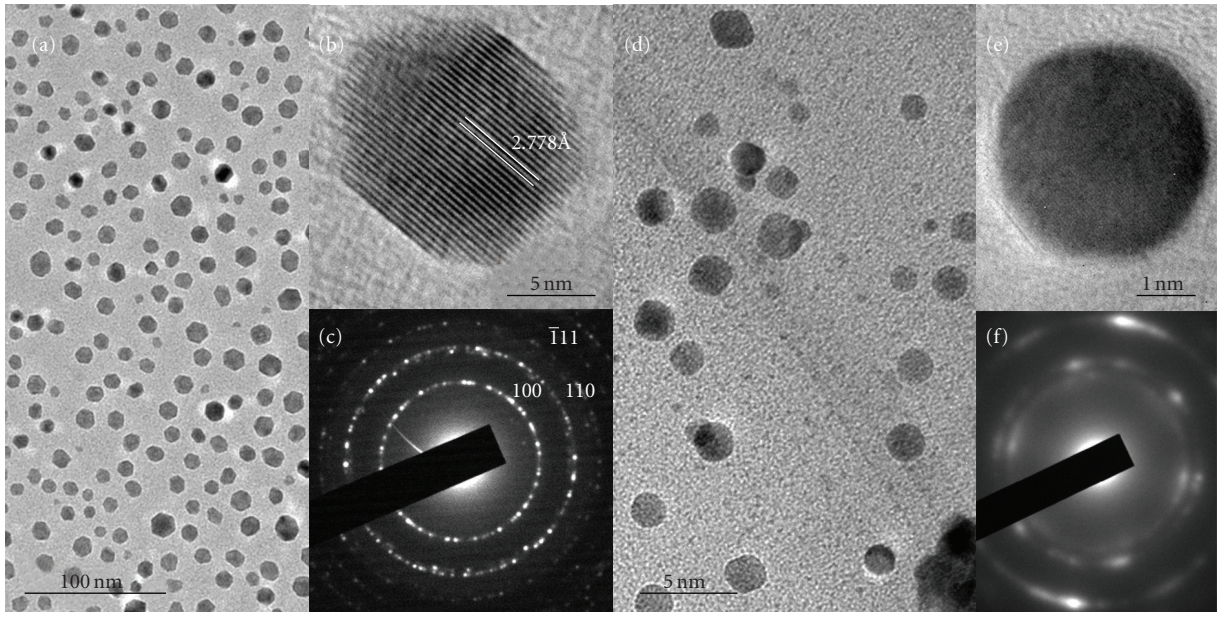

Figure 3: TEM images of $BiFeO_3$ NPs at low and high magnification, and corresponding SAED patterns: (a), (b), and (c) for nanoparticles from tartaric acid and calcined at 450°C, while (d), (e), and (f) for NPs from citric acid and calcined at 350°C.

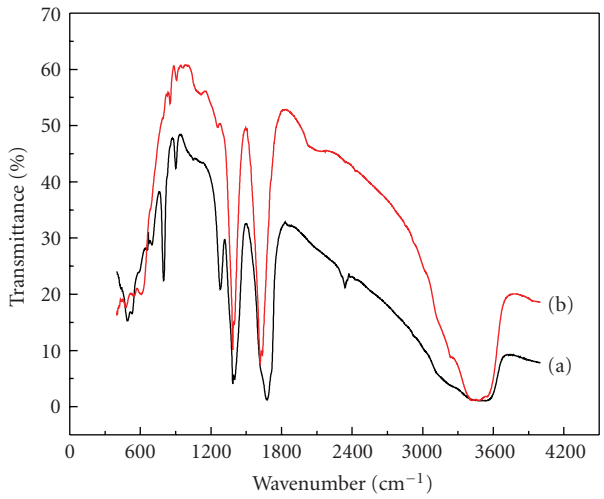

Figure 4: FTIR spectra of $BiFeO_3$ precursors formed by tartaric acid (a) and citric acid (b), respectively.

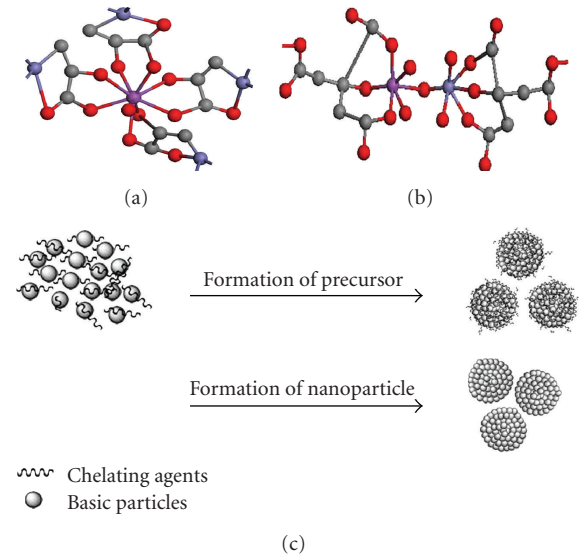

Figure 5: Schematic for different chelating complex formed by tartaric acid (a) and citric acid (b), where purple stands for Bi, blue for Fe, red for oxygen, and gray for carbon atoms. (c) Possible formation processes of $BiFeO_3$ NPs under wet chemical environment using tartaric acid and citric acid as chelating agents, respectively.

(which can be inferred from FRIR spectra of BFO precursors using tartaric and citric acid as chelating, as shown in Figure 4). Finally, the precursor decomposed and BFO NPs started to generate accompanied by the calcination stage under different temperature. It is believed that the chelating compounds plays an important role in controlling shape and size of particles and the decomposition temperatures of the precursor will partially determine the crystallization temperature of BFO NPs in our synthesis. The investigations show that the grain size of the BFO NPs increases with increasing calcination temperature, implying a facile way to BFO NPs with controllable sizes. The geometry of the grains becomes more complicated with higher temperature, a result of better crystallization under high temperature. Higher temperatures cause the grains to grow much bigger so that we can obtain sharper monocrystal SAED image as shown in Figure 6.

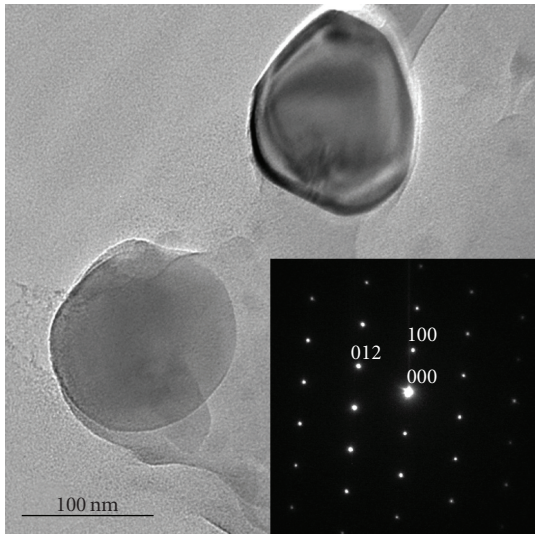

Figure 6: TEM image of $BiFeO_3$ NPs calcined at 650°C and the corresponding SAED pattern (inset), indicated by the black square.

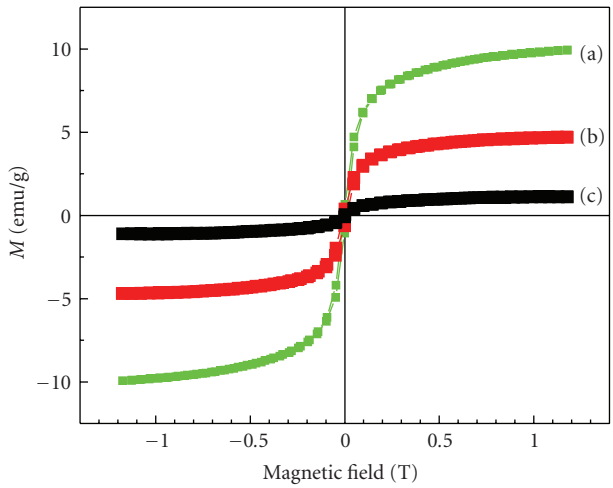

Figure 7: Magnetization hysteresis loops of $BiFeO_3$ NPs with different particle size distributions. (a) 4 nm, (b) 12 nm, and (c) 30 nm.

The magnetization hysteresis loops of BFO NPs samples with three different particle sizes were measured over ±1 T at room temperature, as shown in Figure 7. All loops exhibit a finite exchange bias field and vertical asymmetry with visibly greater saturation magnetizations compared to what has been reported previously [21]. This could be a result of uniform particle sizes and the additional lattice strains caused by the large amount of surfaced atoms from small grain size [28]. According to the theory of BFO's ferromagnetism, magnetization drops as its grain size increases [21]. As the calcination temperature raises, the magnetization of BFO NPs with diameters of 12 and 30 nm decreases as expected. One possible explanation may be that some grains may not have spontaneous magnetic moments and therefore fail to contribute to the magnetization. The possibility of superparamagnetic behaviors in BFO NPs can be ruled out from the finite coercivity and the finite exchange bias field at room temperature (varies within 60 to 90 Oe), which confirms the ferromagnetic order as well as spin pinning at the ferromagnetic—antiferromagnetic interfaces [28]. The magnetization is nearly linear with the external magnetic field for the sample heat treatment at 650°C, which means the NPs has almost lost its ferromagnetic property (the result is not shown here). This finding matches well with what have been found previously, that is, crystallites larger than 62 nm display bulk lattice parameters and hence do not present any ferromagnetic property, namely, the hysteresis loop.

4. Conclusions

In summary, pure phase BFO NPs with an average diameters ranging from 4 to 30 nm were synthesized by a simple soft chemical route using citric acid as chelating agent followed by calcination at a relatively low temperature. TG/DSC, XRD, and TEM were used to confirm the phase and size distribution of the nanoparticles and VSM was utilized to measure the size-dependent magnetic behaviors of the as-prepared nanoparticles. Precursors of the nanoparticles in the experiments as well as the formation mechanism are proposed. This method avoids using traditional high temperature and therefore could be easily extended to other systems.

Acknowledgments

This paper was financially supported by the Research Grants Council of Hong Kong (GRF no.PolyU 5309/08E), and the National Science Foundation of China (NSFC) (Grant nos. 50902046, 50872031). Support from the Center for Smart Materials of the Hong Kong Polytechnic University is also acknowledged.

References

[1] W. Eerenstein, N. D. Mathur, and J. F. Scott, "Multiferroic and magnetoelectric materials," *Nature*, vol. 442, no. 7104, pp. 759–765, 2006.

[2] P. Fischer, M. Polomska, I. Sosnowska, and M. Szymanski, "Temperature dependence of the crystal and magnetic structures of $BiFeO_3$," *Journal of Physics C*, vol. 13, no. 10, pp. 1931–1940, 1980.

[3] C. Tabares-Munoz, J. P. Rivera, A. Monnier, and H. Schmid, "Measurement of the quadratic magnetoelectric effect on single crystalline $BiFeO_3$," *Japanese Journal of Applied Physics*, vol. 24, pp. 1051–1053, 1985.

[4] Y. P. Wang, L. Zhou, M. F. Zhang, X. Y. Chen, J.-M. Liu, and Z. G. Liu, "Room-temperature saturated ferroelectric polarization in $BiFeO_3$ ceramics synthesized by rapid liquid phase sintering," *Applied Physics Letters*, vol. 84, no. 10, pp. 1731–1733, 2004.

[5] M. Fiebig, T. H. Lottermoser, D. Fröhlich, A. V. Goltsev, and R. V. Pisarev, "Observation of coupled magnetic and electric domains," *Nature*, vol. 419, no. 6909, pp. 818–820, 2002.

[6] N. Hur, S. Park, P. A. Sharma, J. S. Ahn, S. Guha, and S.-W. Cheong, "Electric polarization reversal and memory in a multiferroic material induced by magnetic fields," *Nature*, vol. 429, no. 6990, pp. 392–395, 2004.

[7] J. Wang, J. B. Neaton, H. Zheng et al., "Epitaxial $BiFeO_3$ multiferroic thin film heterostructures," *Science*, vol. 299, no. 5613, pp. 1719–1722, 2003.

[8] H. W. Jang, D. Ortiz, S.-H. Baek et al., "Domain engineering for enhanced ferroelectric properties of epitaxial (001) $BiFeO_3$ thin films," *Advanced Materials*, vol. 21, no. 7, pp. 817–823, 2009.

[9] S. K. Singh, Y. K. Kim, H. Funakubo, and H. Ishiwara, "Epitaxial $BiFeO_3$ thin films fabricated by chemical solution deposition," *Applied Physics Letters*, vol. 88, no. 16, Article ID 162904, 2006.

[10] Y. Wang, Q. H. Yang, H. C. He, and C.-W. Nan, "Enhanced ferroelectricity in Ti-doped multiferroic $BiFeO_3$ thin films," *Applied Physics Letters*, vol. 89, no. 5, Article ID 052903, 2006.

[11] Y.-H. Lee, J.-M. Wu, Y.-C. Chen, Y.-H. Lu, and H.-N. Lin, "Surface chemistry and nanoscale characterizations of multiferroic $BiFeO_3$ thin films," *Electrochemical and Solid-State Letters*, vol. 8, no. 10, pp. F43–F46, 2005.

[12] Z. J. Shen, W. P. Chen, G. L. Yuan, J. M. Liu, Y. Wang, and H. L. W. Chan, "Hydrogen-induced degradation in multiferroic $BiFeO_3$ ceramics," *Materials Letters*, vol. 61, no. 22, pp. 4354–4357, 2007.

[13] Z. Yan, K. F. Wang, J. F. Qu, Y. Wang, Z. T. Song, and S. L. Feng, "Processing and properties of Yb-doped $BiFeO_3$ ceramics," *Applied Physics Letters*, vol. 91, no. 8, Article ID 082906, 2007.

[14] U. A. Joshi, J. S. Jang, P. H. Borse, and J. S. Lee, "Microwave synthesis of single-crystalline perovskite $BiFeO_3$ nanocubes for photoelectrode and photocatalytic applications," *Applied Physics Letters*, vol. 92, no. 24, Article ID 242106, 2008.

[15] J. Chen, X. Xing, A. Watson et al., "Rapid synthesis of multiferroic $BiFeO_3$ single-crystalline nanostructures," *Chemistry of Materials*, vol. 19, no. 15, pp. 3598–3600, 2007.

[16] Y. Wang, G. Xu, Z. Ren et al., "Mineralizer-assisted hydrothermal synthesis and characterization of $BiFeO_3$ nanoparticles," *Journal of the American Ceramic Society*, vol. 90, no. 8, pp. 2615–2617, 2007.

[17] J. Wei and D. Xue, "Low-temperature synthesis of $BiFeO_3$ nanoparticles by ethylenediaminetetraacetic acid complexing sol-gel process," *Materials Research Bulletin*, vol. 43, no. 12, pp. 3368–3373, 2008.

[18] X.-L. Yu, Y. Wang, Y.-M. Hu, C.-B. Cao, and H. L.-W. Chan, "Gas-sensing properties of perovskite $BiFeO_3$ nanoparticles," *Journal of the American Ceramic Society*, vol. 92, no. 12, pp. 3105–3107, 2009.

[19] C. M. Cho, J. H. Noh, I.-S. Cho, J.-S. An, K. S. Hong, and J. Y. Kim, "Low-temperature hydrothermal synthesis of pure $BiFeO_3$ nanopowders using triethanolamine and their applications as visible-light photocatalysts," *Journal of the American Ceramic Society*, vol. 91, no. 11, pp. 3753–3755, 2008.

[20] S. Li, Y.-H. Lin, B.-P. Zhang, C.-W. Nan, and Y. Wang, "Photocatalytic and magnetic behaviors observed in nanostructured $BiFeO_3$ particles," *Journal of Applied Physics*, vol. 105, no. 5, Article ID 056105, 2009.

[21] T.-J. Park, G. C. Papaefthymiou, A. J. Viescas, A. R. Moodenbaugh, and S. S. Wong, "Size-dependent magnetic properties of single-crystalline multiferroic $BiFeO_3$ nanoparticles," *Nano Letters*, vol. 7, no. 3, pp. 766–772, 2007.

[22] S. Chattopadhyay, S. D. Kelly, V. R. Palkar, L. Fan, and C. U. Segre, "Investigation of size effects in magnetoelectric $BiFeO_3$," *Physica Scripta*, vol. T115, pp. 709–713, 2005.

[23] S. Ghosh, S. Dasgupta, A. Sen, and H. S. Maiti, "Low temperature synthesis of bismuth ferrite nanoparticles by a ferrioxalate precursor method," *Materials Research Bulletin*, vol. 40, no. 12, pp. 2073–2079, 2005.

[24] J.-T. Han, Y.-H. Huang, X.-J. Wu et al., "Tunable synthesis of bismuth ferrites with various morphologies," *Advanced Materials*, vol. 18, no. 16, pp. 2145–2148, 2006.

[25] C. Chen, J. Cheng, S. Yu, L. Che, and Z. Meng, "Hydrothermal synthesis of perovskite bismuth ferrite crystallites," *Journal of Crystal Growth*, vol. 291, no. 1, pp. 135–139, 2006.

[26] S. M. Selbach, T. Tybell, M.-A. Einarsrud, and T. Grande, "Size-dependent properties of multiferroic $BiFeO_3$ nanoparticles," *Chemistry of Materials*, vol. 19, no. 26, pp. 6478–6484, 2007.

[27] S. Ghosh, S. Dasgupta, A. Sen, and H. S. Maiti, "Low-temperature synthesis of nanosized bismuth ferrite by soft chemical route," *Journal of the American Ceramic Society*, vol. 88, no. 5, pp. 1349–1352, 2005.

[28] R. Mazumder, P. Sujatha Devi, D. Bhattacharya, P. Choudhury, A. Sen, and M. Raja, "Ferromagnetism in nanoscale $BiFeO_3$," *Applied Physics Letters*, vol. 91, no. 6, Article ID 062510, 3 pages, 2007.